EBioMedicine 52 (2020) 102625

Contents lists available at ScienceDirect

EBioMedicine

journal homepage: www.elsevier.com/locate/ebiom

Research paper

DuoBody-CD3xCD20 induces potent T-cell-mediated killing of malignant B cells in preclinical models and provides opportunities for subcutaneous dosing

Patrick J. Engelberts[a,2], Ida H. Hiemstra[a,2], Bart de Jong[a], Danita H. Schuurhuis[a], Joyce Meesters[a], Irati Beltran Hernandez[a], Simone C. Oostindie[a,b], Joost Neijssen[a], Edward N. van den Brink[a], G. Jean Horbach[a], Sandra Verploegen[a], Aran F. Labrijn[a], Theodora Salcedo[a], Janine Schuurman[a], Paul W.H.I Parren[a,b,1], Esther C.W. Breij[a,*]

[a] Genmab, Utrecht, The Netherlands
[b] Dept of Immunohematology and Blood Transfusion, Leiden University Medical Center, Leiden, The Netherlands

ARTICLE INFO

Article History:
Received 12 September 2019
Revised 20 December 2019
Accepted 26 December 2019
Available online xxx

Keywords:
Bispecific antibody
CD3
CD20
T cell redirection
B cell malignancy
Subcutaneous administration

ABSTRACT

Background: DuoBody®-CD3xCD20 (GEN3013) is a full-length human IgG1 bispecific antibody (bsAb) recognizing CD3 and CD20, generated by controlled Fab-arm exchange. Its Fc domain was silenced by introduction of mutations L234F L235E D265A.
Methods: T-cell activation and T-cell-mediated cytotoxicity were measured by flow cytometry following co-culture with tumour cells. Anti-tumour activity of DuoBody-CD3xCD20 was assessed in humanized mouse models *in vivo*. Non-clinical safety studies were performed in cynomolgus monkeys.
Findings: DuoBody-CD3xCD20 induced highly potent T-cell activation and T-cell-mediated cytotoxicity towards malignant B cells *in vitro*. Comparison of DuoBody-CD3xCD20 to CD3 bsAb targeting alternative B-cell antigens, or to CD3xCD20 bsAb generated using alternative CD20 Ab, emphasized its exceptional potency. *In vitro* comparison with other CD3xCD20 bsAb in clinical development showed that DuoBody-CD3xCD20 was significantly more potent than three other bsAb with single CD3 and CD20 binding regions and equally potent as a bsAb with a single CD3 and two CD20 binding regions. DuoBody-CD3xCD20 showed promising anti-tumour activity *in vivo*, also in the presence of excess levels of a CD20 Ab that competes for binding. In cynomolgus monkeys, DuoBody-CD3xCD20 demonstrated profound and long-lasting B-cell depletion from peripheral blood and lymphoid organs, which was comparable after subcutaneous and intravenous administration. Peak plasma levels of DuoBody-CD3xCD20 were lower and delayed after subcutaneous administration, which was associated with a reduction in plasma cytokine levels compared to intravenous administration, while bioavailability was comparable.
Interpretation: Based on these preclinical studies, a clinical trial was initiated to assess the clinical safety of subcutaneous DuoBody-CD3xCD20 in patients with B-cell malignancies.
Funding: Genmab

1. Introduction

Targeting of CD20-expressing cells with CD20-specific monoclonal antibodies (mAb) has shown to be highly successful for the treatment of B-cell malignancies and specific autoimmune diseases. Rituximab was the first CD20-specific mAb to obtain regulatory approval and has rapidly become a key part of the standard of care for both non-Hodgkin's lymphoma and B-cell chronic lymphocytic leukaemia patients. Rituximab is also used in CD20-positive B-lineage acute lymphoblastic leukaemia (B-ALL) [1,2]. Nevertheless, disease relapse or recurrence occurs in many patients [3]. Since resistance of B-cell malignancies to CD20-targeting mAb is rarely caused by loss of CD20 expression or CD20 mutations [4,5], CD20 remains an attractive tumour target, due to its restricted normal tissue expression and prevalent expression on malignant B cells. However, alternative and more powerful targeting strategies are warranted.

* Corresponding author.
E-mail address: EBJ@genmab.com (E.C.W. Breij).
[1] Current affiliations: Dept of Immunohematology and Blood Transfusion, Leiden University Medical Center, Leiden, The Netherlands and Lava Therapeutics, Utrecht, The Netherlands.
[2] These authors contributed equally to this work.

https://doi.org/10.1016/j.ebiom.2019.102625

Research in context

Evidence before this study

CD20 targeting with monoclonal antibodies (mAb) has been shown to be highly successful for the treatment of B-cell malignancies. Since resistance to CD20-targeting mAb is rarely caused by loss of CD20 expression or CD20 mutations, CD20 remains an attractive tumour target, due to its restricted normal tissue expression and prevalent expression in B-cell malignancies. T-cell-redirecting CD3 bispecific antibodies (bsAb) have begun to deliver their promise in the treatment of cancer. CD3 bsAb trigger T cell kill of tumour cells expressing the target antigen, irrespective of T-cell receptor specificity. Generation of bispecific antibodies using controlled Fab-arm exchange (cFAE) has been shown to be very efficient (yield >95%) and results in stable, fully functional IgG1 bsAb.

Added value of this study

The preclinical studies described here show that DuoBody-CD3xCD20, a CD3 bsAb generated by cFAE, induced T-cell activation and T-cell-mediated cytotoxicity towards CD20-expressing malignant B cells with high potency, which could not be explained by CD20 expression levels or binding characteristics of its CD20-binding Fab arm. In comparison with other CD3xCD20 bsAb in clinical development, DuoBody-CD3xCD20 showed equal or superior potency in functional assays *in vitro*. Furthermore, subcutaneous administration of DuoBody-CD3xCD20 induced profound, long-lasting and reversible B-cell depletion from peripheral blood and lymph nodes in cynomolgus monkeys and resulted in reduced peak plasma cytokine levels compared to intravenous administration, while bioavailability was comparable.

Implications of all the available evidence

The present evidence suggests that DuoBody-CD3xCD20 is a promising agent for treatment of B-cell malignancies. The subcutaneous administration route may provide a method to reduce peak cytokine levels in patients, in addition to a reduced treatment burden for patients and improved resource utilization at the treatment facility. Convenience is increasingly important to patients and health care professionals and systems. Based on results of the preclinical studies described here, a clinical trial to assess the safety and preliminary efficacy of subcutaneous DuoBody-CD3xCD20 (GEN3013) in patients with relapsed, progressive or refractory B-cell lymphoma is currently enrolling patients (GCT3013-01, NCT03625037).

Bispecific antibodies (bsAb) specifically recognizing the T-cell antigen CD3 in addition to a tumour-associated antigen (TAA), CD3 bsAb, have begun to deliver their promise in treatment of cancer. CD3 bsAb are able to efficiently induce cytotoxic synapse formation and target cell kill independent of the T-cell receptor (TCR) specificity [6] by binding to CD3ε (alone or in combination with CD3δ) on T cells and the TAA on tumour cells. Thus far, two CD3 bsAb have been approved and marketed: catumaxomab, recognizing CD3 and EpCAM (withdrawn in Jun-2017) and blinatumomab, recognizing CD3 and CD19. Room for improvement exists in both optimization of the bsAb format, for example by prolonging plasma half-life and improving manufacturability, as well as in expanding the arsenal of TAA that can be used as targets for CD3 bsAb in the clinic.

We previously developed a method to generate whole IgG1 bsAb using controlled Fab-arm exchange (cFAE), termed DuoBody® technology. Here, two parental IgG1 mAb, each with a matched single point mutation in the IgG Fc region, reorganize into full-length bispecific IgG1 molecules upon exposure to controlled manufacturing conditions [7,8]. The cFAE process was shown to be an easy and robust method to generate highly stable bsAb with superior yield compared to other bsAb platforms, both at research and manufacturing scale [9]. Importantly, the method provides the opportunity to generate and screen large and diverse panels of bsAb, to identify bsAb with optimal functional characteristics.

DuoBody-CD3xCD20 (GEN3013) is a bsAb recognizing CD3ε and CD20, that is generated by cFAE of a humanized CD3 mAb and the human CD20 mAb 7D8 [10,11]. The Fc region of DuoBody-CD3xCD20 is silenced by three point mutations that were selected based on functional assays. The capacity of DuoBody-CD3xCD20 to activate T cells and induce lysis of cell lines from B-cell malignancies was tested *in vitro*. With the aim to understand its remarkable potency *in vitro*, DuoBody-CD3xCD20 was compared to a diverse panel of other B-cell targeting CD3 bsAb *in vitro*. Anti-tumour activity of DuoBody-CD3xCD20 was tested *in vivo* in humanized mouse models. The pharmacokinetic (PK) properties and its capacity to induce B-cell depletion, after either intravenous or subcutaneous administration, were assessed in cynomolgus monkeys as part of the non-clinical safety studies.

2. Materials & methods

2.1. Antibodies and cell lines

Commercially available mAb and cell lines used in the experiments are listed in Suppl. Tables 1 and 2, respectively. IgG1 mAb that are listed in Suppl. Table 3 were recombinantly produced [12], with an F405L mutation in all CD3 mAb, a K409R mutation in all TAA-specific mAb [7] and FEA (L234F, L235E and D265A) mutations in both. BsAb were generated by cFAE [8], in some cases using the HIV-1 gp120-specific mAb IgG1-b12 [13] to generate bsAb with one non-binding arm. Binding of the bsAb to their antigens was determined by flow cytometry as described (Suppl. data and methods). Four other CD3xCD20 bsAb were produced based on variable and constant region sequences available from published patent applications and literature (bsAb1: WO2014047231, WO2009018411 [Regeneron Pharmaceuticals]; bsAb2: US20170349657 A1, US20140370013 [Xencor Inc.]; bsAb3: [14], US20060034835 A1, US20140242080 A1, US20150166661 [Genentech Inc.]; bsAb4: US20160075785 A1 [Hoffmann-La Roche]). Binding of these bsAb to their targets, CD3 on healthy donor T cells and CD20 on Daudi cells, was confirmed (data not shown).

2.2. Antibody binding assay

Binding of bsAb to cell surface-expressed antigens was determined by flow cytometry as described [15], using an R-phycoerythrin (R-PE)-labelled detection Ab (Suppl. Table 1) to detect primary Ab binding. Binding was detected using an iQue screener (Intellicyt Corporation, USA), a BD LSRFortessa or a BD Canto II flow cytometer (BD Biosciences, Europe).

Simultaneous binding of bsAb to B and T cells was measured as follows: Heparinized whole blood from a healthy donor was incubated with Ab at 37 °C for 2 h. Cells were washed twice and incubated with mAb specific for CD4 or CD8 and CD19 (Suppl. Table 1) at 4 °C for 30 min. Erythrocytes were lysed by addition of erythrocyte lysis buffer (10 mM $KHCO_3$/0.01 mM EDTA/155 mM NH_4Cl dissolved in dH_2O). Samples were analysed by flow cytometry, using a BD Canto II (BD Biosciences Europe). The number of $CD4^+CD19^+$ or $CD8^+CD19^+$ double-positive events, indicative of simultaneous binding of DuoBody-CD3xCD20 to human T and B cells, was quantified by CD4/CD19 and CD8/CD19 quadrant analysis, after measuring a fixed sample volume.

2.3. Determination of target expression levels (QiFi)

Target expression, in terms of specific antibody-binding capacity (sABC), was measured using the QiFi kit (DAKO) according to manufacturer's instructions. Ab used in these experiments are listed in Suppl. Table 1.

2.4. In vitro *T-cell assays*

Buffy coats from healthy donors (Sanquin, Amsterdam) were used to isolate either peripheral blood mononuclear cells (PBMC) using Lymphocyte separation medium (Lonza, Basel, Switzerland) or pan-T cells, $CD4^+$ T cells or $CD8^+$ *T* cells by negative selection using RosetteSEP™ Enrichment cocktail kits (Stem Cell Technologies, Vancouver, Canada). CD3 bsAb-induced T-cell-mediated cytotoxicity was determined with a chromium release, alamarBlue or flow cytometric assay. Chromium-release assays with isolated T cells and target cells were performed as described [16]. E:T ratios tested are indicated in the Figure legends. Specific lysis was calculated as:% specific lysis = ((CPM sample − CPM background lysis)/(CPM maximal lysis − CPM background lysis)) x 100, where CPM refers to counts per minute. ^{51}Cr release was measured using a gamma counter (Cobra model C5002; Packard-PerkinElmer).

Alternatively, cytotoxicity was measured using flow cytometry: isolated T cells were incubated with bsAb and tumor cell lines (E:T ratio 2:1) for 48 h, or PBMC (containing both effector and target cells) were incubated with bsAb for 72 h. Cells were washed, stained for T- and B-cell markers (Suppl. Table 1), washed again, after which a fixed sample volume was measured on a BD LSRFortessa™ cell analyzer (BD Biosciences, San Jose, CA, USA). Data were analysed using FlowJo® software V10.1 (Ashland, OR, USA). % B-cell lysis was calculated as follows: $100 - ((\text{cell count}_{\text{sample}}/\text{cell count}_{\text{medium}}) \times 100\%)$.

AlamarBlue viability assays were performed to measure T-cell-mediated cytotoxicity towards adherent target cells. Tumor cells were plated in 96-well culture plates and allowed to adhere at 37 °C, 5% CO_2 for at least 3 h. PBMC and Ab were then added to the plates (E:T ratio 1:1). Tumour cells incubated with a 5% (v/v) final concentration of staurosporine (Sigma Aldrich), an inducer of apoptosis, were used as a positive control; tumour cells with medium only, with medium and PBMC or with Ab only were used as negative controls. Plates were incubated at 37 °C, 5% CO_2 for three days, after which plates were washed twice with PBS to remove PBMC, Ab and debris. Fresh culture medium containing 10% alamarBlue® (BioSource International) was added and incubated at 37 °C, 5% CO_2, for 4 h. Tumour cell viability was measured on an EnVision Multilabel Plate Reader (Perkin Elmer).

2.5. Confocal microscopy

Daudi cells were labelled with CellTracker Deep Red (Invitrogen, Carlsbad, California, USA), according to the manufacturer's instructions, seeded on a Cell-Tak-coated (Corning) chamber slide (Thermo Scientific Nunc), incubated at 37 °C for 30 min, followed by incubation with 1 μg/mL DuoBody-CD3xCD20 and T cells (1:1 ratio Daudi:T cells, 24 h). Cells were fixed in 2% formaldehyde at RT for 10 min and stained for CD69 or bound DuoBody-CD3xCD20 at RT for 45 min. Intracellular staining of perforin was performed after the cells were permeabilized with Cytofix/Cytoperm solution (BD Biosciences) at 4 °C for 20 min (antibodies listed in Suppl. Table 1). All samples were washed with PBS and mounted using vectashield (with DAPI, Vector Laboratories). Images were taken with a confocal laser scanning microscope Nikon A1R/STORM and a 60x objective (Apo 60x Oil λS DIC N2). Acquired images were processed with ImageJ [17].

2.6. In vivo *mouse models*

A PBMC co-engraftment xenograft model was performed as described [18]. At day 0, female NOD.C.B-17-Prkdc scid/J (NOD-SCID) mice, 9–10 weeks of age at the moment of tumour cell injection, were inoculated with a mixture of 5×10^6 PBMC and 5×10^6 luciferase-expressing Raji cells (Raji-luc) subcutaneously (SC) on the right flank. Immediately after injection, mice were treated intravenously (IV) with Ab. Since treatment was performed before palpable tumours appeared, animals were picked randomly from the cages and treatment groups were randomized over all cages. BRGS (BALB/c Rag2tm1Fwa IL-2Rγctm1CgnSIRPα.NOD) mice with a humanized immune system (HIS) were generated as described [19]. These humanized mouse models were performed at Axenis (Paris, France). After 14–15 weeks, mice were inoculated with 5×10^6 Daudi-luc (IV) or Raji-luc (SC) cells (day 0 of the study). Mice were randomized based on the number of $CD3^+$ T cells and the $CD34^+$ haematopoietic stem cell donors, and treated IV with Ab, starting at day 3. Tumour growth was evaluated by bioluminescence imaging (BLI) or calliper measurements (tumour volume $[mm^3] = 0.52 \times [\text{length}] \times [\text{width}]^2$). Blood leukocyte cell counts, and activation status were determined by flow cytometry (Ab listed in Suppl. Table 1). Sample sizes for *in vivo* experiments in mice were chosen based on power analysis, the growth characteristics of the tumour model (homogenous *vs.* heterogeneous outgrowth in untreated animals) and the expected efficacy of the drug. Using historical data, growth of five different human xenograft models was compared after SC implantation in mice. From this comparison, the average coefficient of variance (CV) was calculated to be 31% at a mean tumour size of 883 mm^3, at the last day that all groups in the study were intact. Analysis using GraphPad StatMate indicated that group sizes of $n = 10$, $n = 8$ and $n = 6$ indicated a power of 80% for a reduction in tumour growth of 41.4% ($n = 10$), 47% ($n = 8$) and 55.9% ($n = 6$) to be detected with a significance of 0.05. For co-engraftment of Raji cells and PBMC from one donor, sample sizes of $n = 4$ (Fig. 4A) and $n = 5$ (Fig. 4B) were selected. Since two PBMC donors were used in these experiments, a total of $n = 8$ (A) and $n = 10$ (B) mice was used per group. For Fig. 4C-G, a sample size of $n = 8$ was selected.

For PK and clearance analysis of Ab, an analysis was performed using five tests with a total of 80 mice, in which five different Ab were evaluated in different mouse strains. Power analysis indicated that with a group size of $n = 3$, differences of 0.2 in log-clearance could be demonstrated with 80% power. This means that differences can be determined if plasma clearance rate of one Ab is 66% faster or slower than that of another antibody. Practice has shown that changes in Ab structure easily lead to large differences in clearance rate. Therefore, group sizes of $n = 3$ were considered sufficient (Suppl. Fig. 1J). CB17/lcr-Prkdcscid/lcrlcoCrl, female mice were used, 10–11 weeks at the time of Ab injection. At the time of Ab injection for PK studies, animals were picked randomly from the cages and treatment groups were randomized over all cages.

All animal experiments were performed in compliance with European directives (2010/63/EU) and approved by the local Ethical committees. Animals were housed and handled in accordance with good animal practice as defined by FELASA, in an AAALAC and ISO 9001:2000 accredited animal facility (GDL). For experiments performed at Axenis, animal experimental procedures have received an approval form the local animal Ethical Committee (CETEA 89), Institute Pasteur de Paris.

2.7. Non-clinical safety studies in cynomolgus monkeys

Non-clinical safety studies were conducted at Charles River Laboratories (Tranent, UK) in accordance with the European Convention for the Protection of Vertebrate Animals Used for Experimental and Other Scientific Purposes (Council of Europe), under control of the UK Home Office. This facility is a GLP compliant facility and the practices and procedures adopted during the conduct were consistent with the OECD Principles of Good Laboratory Practice as incorporated into the United Kingdom Statutory Instrument for GLP.

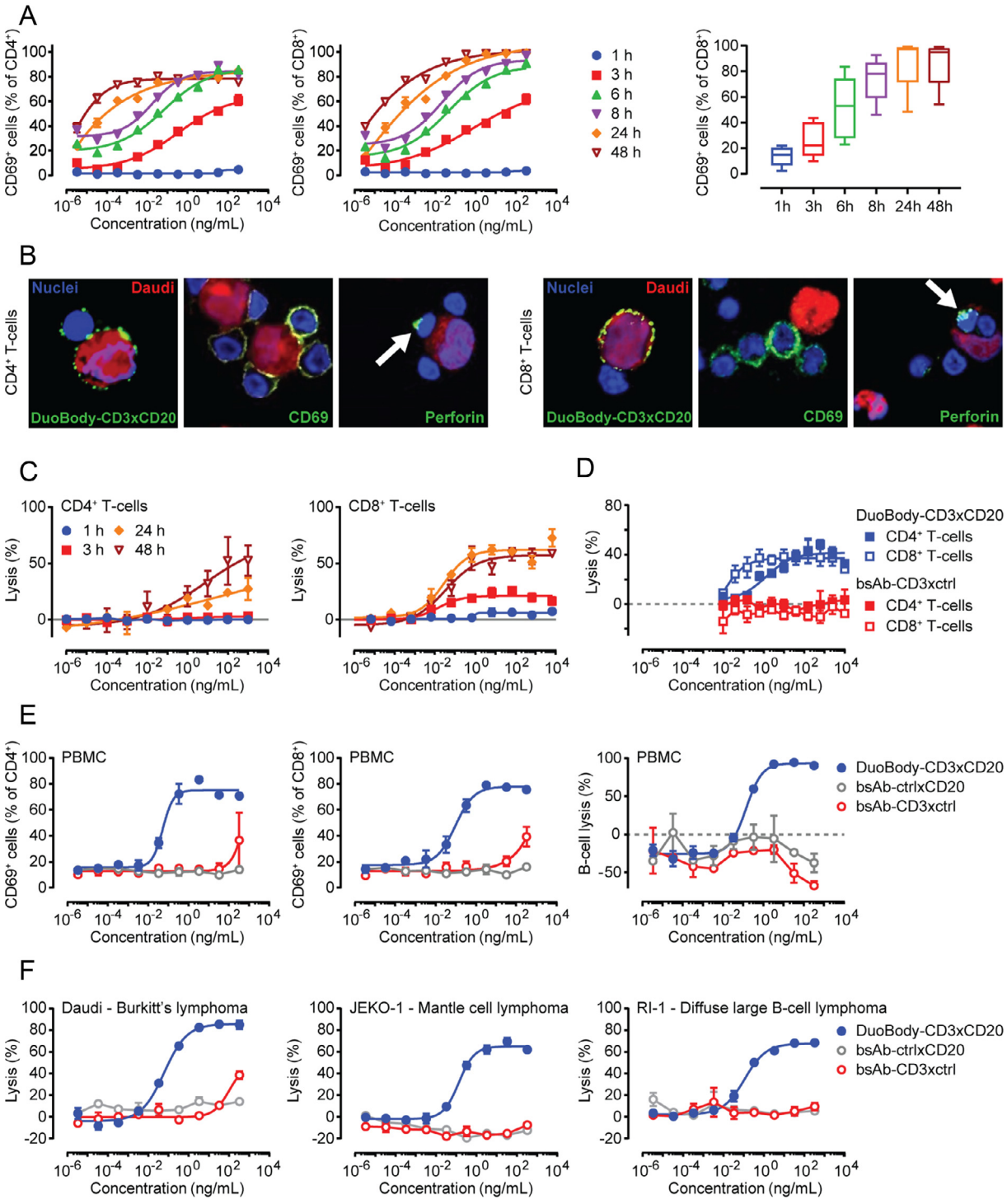

Fig. 1. Functional characterization of DuoBody-CD3xCD20 *in vitro*. **A:** Isolated T cells were incubated with DuoBody-CD3xCD20 and Daudi cells (E:T ratio 2:1). Percentages of CD69-positive CD4$^+$ (**left**) and CD8$^+$ *T* cells (**middle**) were determined by flow cytometry at the indicated time points. Data for one representative donor out of four donors is shown. Graphs show the mean ± standard error of the mean (SEM) of duplicate wells. The **right** panel shows percentages of CD69-positive CD4$^+$ *T* cells. Data shown are pooled data from 6–8 donors for T cells treated with 3.3 ng/mL DuoBody-CD3xCD20. Boxes extend from 25th to 75th percentiles. Whiskers are drawn down to minimum and up to maximum percentages. Median percentages are indicated. A significant linear trend was observed in time (one-way ANOVA with post-test for linear trend). **B:** Isolated T cells were co-cultured with Daudi cells (E:T ratio 1:1) in the presence of 1 μg/mL DuoBody-CD3xCD20 for 24 h. Images were taken at a 60x magnification (plus extra optical magnification of the left pictures) and are representative of three experiments. **C:** Isolated CD4$^+$ (**left**) or CD8$^+$ *T* cells (**right**) were incubated with DuoBody-CD3xCD20 and chromium-labelled Daudi cells (E:T ratio 20:1; this relatively high E:T ratio was chosen to make sure that a signal could be measured for CD4$^+$ *T* cells and at early time points) for the indicated time periods. Data shown are mean percentages of Daudi cell lysis ± SEM of triplicates. Data from one representative donor out of six donors tested is shown. **D:** Isolated CD4$^+$ or CD8$^+$ *T* cells were incubated with DuoBody-CD3xCD20 or bsAb-CD3xctrl and chromium-labelled Daudi cells (E:T ratio 8:1) for 24 h. Data shown are mean percentages of Daudi cell lysis ± SEM of triplicates. Data from one representative experiment out of 3 performed is shown. **E:** PBMC were incubated with indicated Ab for 72 h. Percentages of CD69-positive CD4$^+$ (**left**) and CD8$^+$ *T* cells (**middle**) and the remaining number of intact endogenous B cells (**right**) were determined by flow cytometry. Data shown are from one representative experiment out of four performed and are mean percentages ± SEM of duplicate wells. **F**: Isolated T cells were incubated with DuoBody-CD3xCD20, bsAb-CD3xctrl or bsAb-ctrlxCD20 and indicated B-cell lymphoma cell lines (E:T ratio 2:1) for 48 h. The remaining number of intact lymphoma cells (**right**) were determined by flow cytometry. Data shown for each cell line are from one representative donor (for number of donors tested see Table 1) and are mean percentages ± SEM of duplicate wells.

Cynomolgus monkeys (purpose-bred cynomolgus monkeys [Macaca fascicularis, of Mauritian origin, Fig. 5A-D: 26–29 months old at allocation to the study; 2.65–3.03 kg; 2.71–3.06 kg at dosing; Fig. 5 E-F: 4–6 years at the time of dosing, 3.2–7.9 kg]) received DuoBody-CD3xCD20 either via an IV infusion or a SC injection. Blood samples and lymph node biopsies were taken to determine B-cell counts and concentrations of Ab and cytokines. Single-cell suspensions were prepared from lymph node biopsies using the Medimachine System (Becton Dickinson). The number of B cells in whole blood samples or lymph node biopsies was determined by flow cytometry using a two-laser five-color Beckman Coulter FC500 or a BD LSRFortessa, gating for $CD19^+$ cells (antibodies listed in Suppl. Table 1).

Plasma was isolated from whole blood by centrifugation (1500x*g*, 4 °C, 10 min). DuoBody-CD3xCD20 concentrations were determined with a Single Molecule Counting ImmunoAssay method (PRA, Assen, The Netherlands). Cytokine concentrations were measured using the Milliplex MAP NHP Cytokine Magnetic Bead Panel (Millipore) on a Bio-Plex 200 reader (BioRad).

The numbers of cynomolgus monkeys evaluated in toxicity studies were the minimum required to properly characterise the effects of the test article and to avoid an unnecessary number of animals to accomplish the study objectives. Fig. 5A-D: $n = 2$ female monkeys per group; Fig. 5E-F: $n = 6$ monkeys (3 males and 3 females) per group. For allocation to dose groups, animals were randomly allocated to groups and subsequently assigned individual animal numbers. Individual body weights were reviewed to ensure a balanced distribution across groups. For quantitative numerical data where $n \leq 3$, no statistical analyses were applied. These data were evaluated by comparing the individual data in a descriptive manner.

2.8. Data analysis and statistics

Dose-response curves were generated using four-parameter non-linear regression analysis (GraphPad Prism 7.02 software [La Jolla, CA, USA]; equation log[agonist] *vs.* response – variable slope). Half maximal effective concentration (EC_{50}) values were derived from these curves. In *in vivo* experiments, differences in tumour growth or frequency of cellular subsets were analysed in treated *versus* control mice by Mann-Whitney two-tailed test or by a Kruskal-Wallis analysis of variance [ANOVA] test followed by Dunn's multiple comparison post-test, as indicated.

3. Results

3.1. Selection of mutations to obtain CD3 bsAb with a silenced Fc region

A fully functional IgG1 Fc region that is capable of inducing Fc-mediated effector functions is not desirable for CD3 bsAb, because Ab-dependent Fc gamma receptor (FcγR)-mediated cross-linking of CD3 on T cells may induce TAA-independent T-cell activation and cytotoxicity. In addition, Ab-dependent cell-mediated cytotoxicity (ADCC) and complement-dependent cytotoxicity (CDC), may lead to cytotoxicity towards T cells. Furthermore, we observed ineffective T-cell redirection by an Fc-effector function-competent (active) CD3 bsAb in a syngeneic mouse tumour model [20]. We set out to identify mutations to silence Fc-mediated effector functions, that were compatible with generation of (CD3) bsAb using cFAE. Point mutations N297Q, L234F, L235E, D265A, P331S [21–27], alone or in combination, were introduced in CD3-specific IgG1 mAb or bsAb, and tested for their capacity to prevent FcγR and complement binding, while retaining neonatal FcR (FcRn) binding.

The combination of three mutations L234F, L235E and D265A (FEA) provided the most favourable characteristics *in vitro* and *in vivo*: CD3-specific mAb carrying the FEA mutations showed normal antigen binding (Suppl. Fig. 1A), did not induce Ab-dependent FcγR-mediated T-cell activation or proliferation (Suppl. Fig.1B-C) and did not induce untargeted cytotoxicity in tumour cells (Suppl. Fig. 1D). Similarly, CD3 bsAb carrying the FEA mutations induced cytotoxicity in HER2-expressing tumour cells when the TAA-specific Fab-arm recognized HER2 (Suppl. Fig. 1E-F). CD3 mAb bearing the FEA mutations were unable to bind membrane expressed FcγRI (Suppl. Fig. 1G) and immobilized CD3 mAb with the FEA mutations had lost the capacity to bind FcγRII, FcγRIII (data not shown) and complement component C1q (Suppl. Fig. 1H). CD3 mAb with the FEA mutations showed normal binding to human and mouse FcRn *in vitro* (data not shown) and demonstrated a normal plasma half-life *in vivo* (Suppl. Fig.1I-J). Finally, introduction of the FEA mutations did not have impact on the efficiency of cFAE (data not shown).

3.2. Functional characterization of DuoBody-CD3xCD20 in vitro

DuoBody-CD3xCD20 was generated by cFAE of a humanized variant of the mouse anti-human CD3 mAb SP34 [28] and the human anti-CD20 mAb IgG1-7D8 [10,11], carrying the matched DuoBody mutations F405L and K409R (respectively) and the FEA mutations.

DuoBody-CD3xCD20 induced dose-dependent activation of $CD4^+$ and $CD8^+$ *T* cells upon incubation in the presence of CD20-expressing Daudi cells, as assessed by upregulation of CD69 (Fig. 1A) and CD25 (Suppl. Fig. 2A), with comparable kinetics for $CD4^+$ and $CD8^+$ *T* cells. The capacity of DuoBody-CD3xCD20 to activate T cells was confirmed by confocal microscopy. In addition to the presence of CD69 on $CD4^+$ and $CD8^+$ *T* cells, perforin, a component of cytotoxic granules, was detected in T cells that were near Daudi cells (Fig. 1B). DuoBody-CD3xCD20 induced potent dose-dependent T-cell-mediated cytotoxicity towards Daudi cells. In contrast to the kinetics of T-cell activation, the kinetics of DuoBody-CD3xCD20-induced tumour cell kill were different for $CD4^+$ and $CD8^+$ *T* cells. While $CD8^+$ *T*-cell-mediated cytotoxicity was already measurable after 3 h, $CD4^+$ *T*-cell-mediated cytotoxicity could not be detected at that time point (Fig. 1C). Furthermore, at the same effector to target cell (E:T) ratio, $CD8^+$ *T* cells induced more efficient target cell lysis than $CD4^+$ *T* cells (Fig. 1D).

Selective targeting of CD20-positive cells by DuoBody-CD3xCD20 was confirmed in healthy donor PBMC, that contain both CD3-expressing effector cells and CD20-expressing target cells. Flow cytometry experiments demonstrated formation of CD4/CD19 and CD8/CD19 double-positive events, indicative of T/B-cell doublets, in the presence of DuoBody-CD3xCD20 (Suppl. Fig. 2B). This demonstrates that DuoBody-CD3xCD20 can simultaneously bind B and T cells. Moreover, DuoBody-CD3xCD20 induced activation of both $CD4^+$ and $CD8^+$ *T* cells and subsequent lysis of normal B cells in PBMC, as assessed by flow cytometry after 72 h of incubation (Table 1, Fig. 1E). Both T-cell activation and cytotoxicity strictly required simultaneous binding of CD3 and CD20, since bsAb controls bsAb-CD3xctrl and bsAb-ctrlxCD20 did not induce T-cell activation or B-cell depletion (Fig. 1E) in PBMC.

The capacity of DuoBody-CD3xCD20 to induce cytotoxicity in malignant B cells was further analysed in a panel of cell lines derived from various types of B-cell lymphoma, with CD20 cell surface expression ranging from 33,000–350,000 specific antibody-binding capacity (sABC). DuoBody-CD3xCD20 induced potent cytotoxicity in all cell lines tested, with EC_{50} values in the low picomolar range. There was no relation between antigen expression and cytotoxicity, suggesting that antigen expression of 33,000 CD20 molecules per cell is sufficient to achieve maximal T-cell-mediated cytotoxicity in the presence of DuoBody-CD3xCD20 (Table 1, Fig. 1F).

In summary, DuoBody-CD3xCD20 induced highly potent kill of CD20-positive tumour cells, which was mediated by both $CD4^+$ and $CD8^+$ *T* cells. T-cell activation and cytotoxic activity were strictly dependent on binding of both CD3 and CD20.

Table 1
Average EC_{50} values of DuoBody-CD3xCD20-induced cytotoxicity. Averages of CD20 expression levels and EC_{50} values of DuoBody-CD3xCD20-induced T-cell-mediated cytotoxicity and T-cell activation (% CD69 positive cells) measurements for each B-cell lymphoma cell line tested, calculated from multiple experiments. CD20 expression levels were determined by quantitative flow cytometry (QiFi) and shown as sABC. EC_{50} values were calculated from flow cytometry-based cytotoxicity assays at E:T ratio 2:1 (% kill;% CD69-positive after 48-h incubation). (GCB = germinal centre B-cell diffuse large B-cell lymphoma, ABC = activated B-cell diffuse large B-cell lymphoma, BL = Burkitt's lymphoma, MCL = mantle-cell lymphoma, *n* = the number of donors with complete dose-response curves or number of tests performed).

Cell line		CD20-expression level (sABC/cell)			DuoBody-CD3xCD20-induced cytotoxicity (average EC_{50} [SD])			DuoBody-CD3xCD20-induced $CD4^+$ T-cell activation (%CD69-pos; average EC_{50} [SD])			DuoBody-CD3xCD20-induced $CD8^+$ T-cell activation (%CD69-pos; average EC_{50} [SD])		
Name	Lymphoma type	Average (x1,000)	Range (x1,000)	n tests	ng/mL	pM	n donors	ng/mL	pM	n donors	ng/mL	pM	n donors
OCI-Ly7	GCB	350	209–453	6	0.531 [0.813]	3.540 [5.420]	3	0.048 [0.051]	0.320 [0.340]	6	0.121 [0.195]	0.807 [1.300]	6
Daudi	BL	331	97–752	11	0.039 [0.022]	0.260 [0.147]	11	0.011 [0.020]	0.073 [0.133]	10	0.025 [0.020]	0.167 [0.133]	10
SU-DHL-4	GCB	308	101–715	7	0.031 [0.000]	0.207 [0.000]	2	0.025 [0.034]	0.167 [0.227]	8	0.097 [0.213]	0.647 [1.420]	10
RI-1	ABC	240	150–356	4	0.066 [0.083]	0.440 [0.553]	6	0.010 [0.015]	0.067 [0.100]	7	0.014 [0.017]	0.093 [0.113]	6
JEKO-1	MCL	233	159–276	3	0.089 [0.033]	0.593 [0.220]	4	0.014 [0.021]	0.093 [0.140]	6	0.204 [0.478]	1.360 [3.187]	6
WSU-DLCL2	GCB	233	144–330	4	0.116 [0.030]	0.773 [0.200]	4	0.050 [0.053]	0.333 [0.353]	4	0.129 [0.077]	0.860 [0.513]	4
U-2932	ABC	180	85–241	4	67.604 [114.929]	450.693 [766.193]	4	0.009 [0.012]	0.060 [0.080]	11	0.009 [0.013]	0.060 [0.087]	10
OCI-Ly18	GCB	166	84–237	4	0.057 [0.042]	0.380 [0.280]	3	0.015 [0.013]	0.100 [0.087]	3	0.028 [0.022]	0.187 [0.147]	3
RC-K8	ABC	139	78–223	4	0.743 [0.673]	4.953 [4.487]	2	0.008 [0.002]	0.053 [0.013]	2	0.040 [0.012]	0.267 [0.080]	2
Z-138	MCL	90	53–114	5	0.057 [0.023]	0.380 [0.153]	2	0.004 [0.007]	0.027 [0.047]	3	0.017 [0.013]	0.113 [0.087]	3
OCI-Ly19	GCB	36	0–62	4	0.181 [0.086]	1.207 [0.573]	2	0.001 [0.001]	0.007 [0.007]	6	0.002 [0.003]	0.013 [0.020]	6
SU-DHL-8	GCB	33	0–88	8	0.120 [0.105]	0.800 [0.700]	2	0.001 [0.000]	0.006 [0.002]	2	0.001 [0.000]	0.003 [0.001]	2

3.3. Assessment of the contribution of the B-cell-targeting Fab arm to CD3 bsAb efficacy in vitro

The CD20-specific Fab arm of DuoBody-CD3xCD20 was derived from the previously described CD20-specific human IgG1-7D8 [10,11]. To study the contribution of this specific Fab arm to the observed potency of DuoBody-CD3xCD20, we compared the capacity to induce T-cell-mediated cytotoxicity of a CD3 bsAb based on 7D8, with CD3 bsAb using B-cell-targeting arms derived from mAb against seven other well-known B-cell membrane molecules: CD22, CD24, CD37, CD70, CD79b, CD138 and human leukocyte antigen (HLA)-DR. CD3 bsAb targeting the different tumour antigens showed strong variation in cytotoxic capacity, as demonstrated in a 24-h chromium release assay, and cytotoxicity did not correlate with antigen expression levels (Fig. 2**A**). The CD20-specific CD3 bsAb (generated using a 7D8-derived Fab arm) was among the most potent CD3 bsAb. Interestingly, none of CD3 bsAb targeting HLA-DR or CD138, both of which show antigen expression levels comparable to or higher than CD20, were able to induce cytotoxicity, demonstrating that high levels of antigen expression do not guarantee efficacy of CD3 bsAb.

In a next set of experiments, CD20, in addition to CD37 and CD70, the three antigens that were most efficiently targeted with CD3 bsAb in the first experiment, were used to assess the contribution of binding characteristics of the TAA-specific Fab-arm to CD3 bsAb-induced cytotoxicity. DuoBody-CD3xCD20 was compared with three other CD20-specific CD3 bsAb and, similarly, four different CD3 bsAb targeting CD37 and CD70 were generated and compared. The tumour-targeting Fab arms were selected based on diversity in binding epitopes ([29,30] and Suppl. Table 4) and target antigen-binding characteristics (EC_{50} and maximal binding), as assessed by flow cytometry (Fig. 2B).

Binding characteristics of the TAA-binding Fab arm (Fig. 2B) did not predict the capacity of CD3 bsAb to induce T-cell-mediated cytotoxicity (Fig. 2C) in experiments using Daudi cells as target cells and purified healthy donor T cells as effector cells. Despite the difference in EC_{50} and maximal binding of $CD3xCD20_{2C6}$ compared to $CD3xCD20_{hu2H7}$ and $CD3xCD20_{Ritux}$, all three bsAb displayed comparable cytotoxic activity in Daudi cells. DuoBody-CD3xCD20, while demonstrating lower apparent affinity than $CD3xCD20_{2C6}$, demonstrated higher maximum levels of binding and considerably more potent cytotoxicity. The CD37-targeting CD3 bsAb, $CD3xCD37_{Ab3}$, $CD3xCD37_{Ab5}$ and $CD3xCD37_{Ab6}$ also showed considerable differences in maximal antigen binding but induced comparable cytotoxicity. $CD3xCD37_{Ab4}$ showed reduced binding, and reduced potency compared to the other CD3xCD37 bsAb. For the CD70 bsAb, the potency observed for Daudi cells was considerably lower than for RPMI-8226 cells that were used in the first experiment (Fig. 2A), despite higher expression of CD70 on Daudi cells (RPMI-8226: 3,900 sABC, Daudi: 12,900 sABC). Nonetheless, also for CD70, the differences in potency of CD3 bsAb could not be predicted based on the binding characteristics.

Taken together, while the CD20-specific Fab arm derived from IgG1-7D8 determines the unique potency of DuoBody-CD3xCD20, neither TAA expression levels nor the TAA binding characteristics could predict the potency of B-cell-specific CD3 bsAb *in vitro*.

Finally, the potency of DuoBody-CD3xCD20 *in vitro* was compared to four other, previously described, CD3xCD20 bsAb that are currently being evaluated in the clinic (sequences and format specifics were obtained from patent applications). The capacity of these bsAb to induce T-cell activation (Fig. 3A-B) and T-cell-mediated cytotoxicity (Fig. 3C) was analysed by incubation with isolated T cells and Daudi cells for 48 h. DuoBody-CD3xCD20 was found to be significantly more potent than three IgG1-like bsAb with a single CD3 and CD20 binding region, and equally potent as a bsAb with a single CD3 and two CD20 binding regions (Fig. 3D).

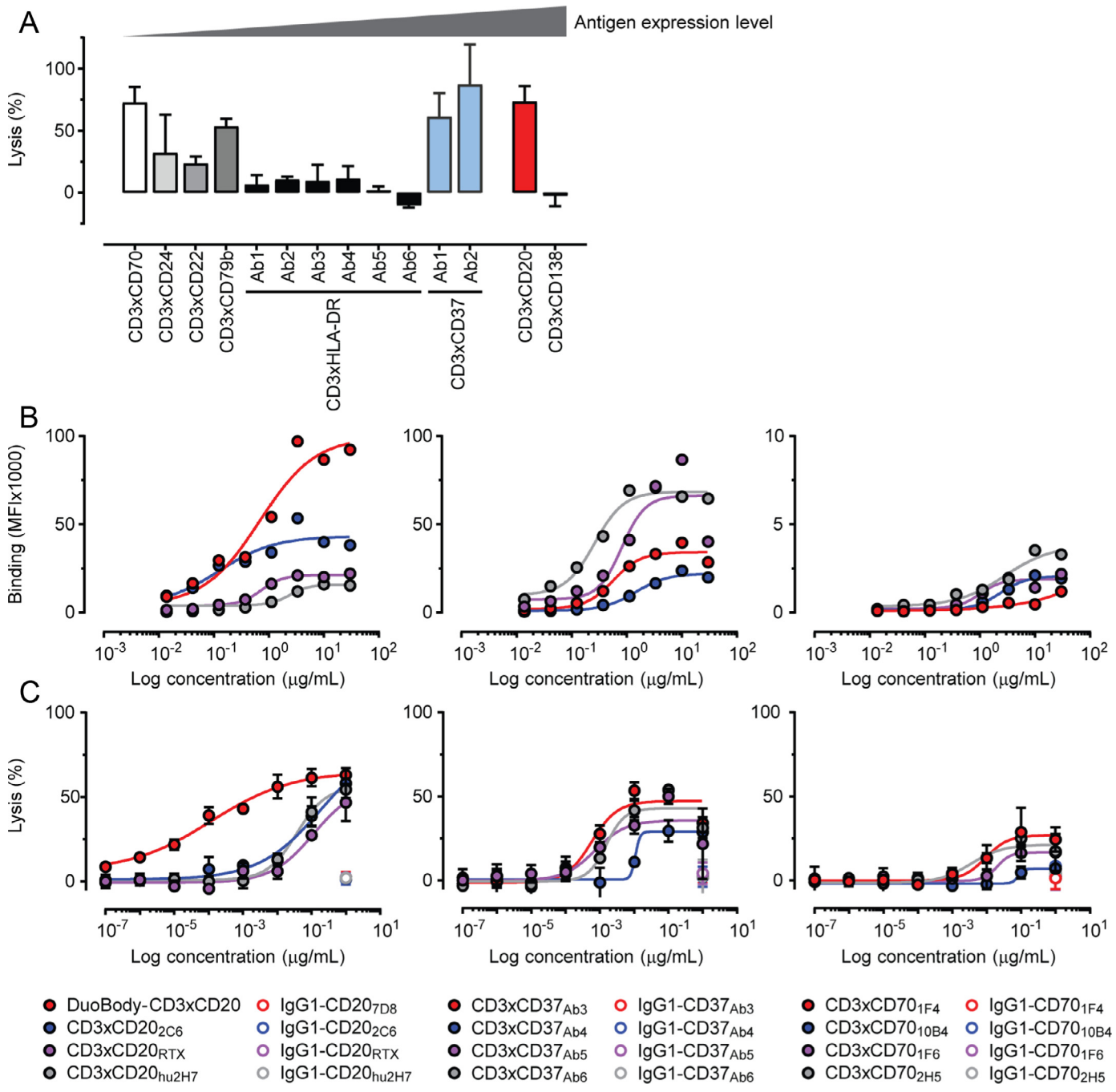

Fig. 2. Assessment of the contribution of the B-cell-targeting Fab arm to CD3 bsAb efficacy *in vitro*. **A:** CD3 bsAb targeting eight different B-cell antigens were added at a concentration of 1 μg/mL to a coculture of purified T cells and chromium-loaded target cells (E:T ratio 10:1). Target cell lysis was measured by chromium release after 24 h. The B-cell antigens are depicted in order from lowest to highest expression level on the B-cell line used as target cell in the assay (CD70: 3,900 sABC on RPMI-8226; CD24: 4,000 sABC on RPMI-8226; CD22: 16,000 sABC on RI-1; CD79b: 111,000 sABC on Daudi; HLA-DR: 205,000 sABC on Daudi; CD37: 224,000 sABC on OCI-Ly7; CD20: 240,000 sABC on RI-1, CD138: 697,000 sABC on RPMI-8226; as determined by QiFi analysis). Experiments were performed twice in triplicates, with two different T-cell donors per experiment (except for CD3xCD37: one experiment with two donors; CD3xCD20: three experiments with two donors; CD3xCD38: two experiments with two donors and one experiment with one donor). Figure shows the mean ± SD for one donor from one representative experiment performed in triplicate. **B:** Binding of indicated CD3xCD20 (**left**), CD3xCD37 (**middle**) and CD3xCD70 (**right**) bsAb to their TAA on Daudi cells was measured by flow cytometry. Data is shown as mean fluorescence intensities (MFI). Graphs show one representative experiment out of 2 (CD3xCD37, CD3xCD70) or 3 (CD3xCD20) performed. **C:** Isolated T cells were incubated with indicated CD3 bsAb or control Ab (as indicated) and chromium-labelled Daudi cells (E:T ratio 10:1) for 24 h. T-cell-mediated cytotoxicity is shown as the mean percentage of Daudi cell lysis ± SEM of triplicates. One representative donor out of 4 donors tested in 2 separate experiments is shown.

3.4. DuoBody-CD3xCD20 induced potent anti-tumour activity in humanized mouse models

The anti-tumour activity of DuoBody-CD3xCD20 was assessed *in vivo* using CD20-positive lymphoma xenograft models in mice engrafted with human immune cells. In a co-engraftment model where NOD-SCID mice were injected SC with a 1:1 mixture of PBMC and Raji B-cell lymphoma cells, followed by IV administration of Ab 2 h later, DuoBody-CD3xCD20 induced a dose-dependent decrease in tumour outgrowth compared to phosphate-buffered saline (PBS) (Fig. 4**A**). In the same model, we assessed the capacity of DuoBody-CD3xCD20 to exert anti-tumour activity in the presence of circulating

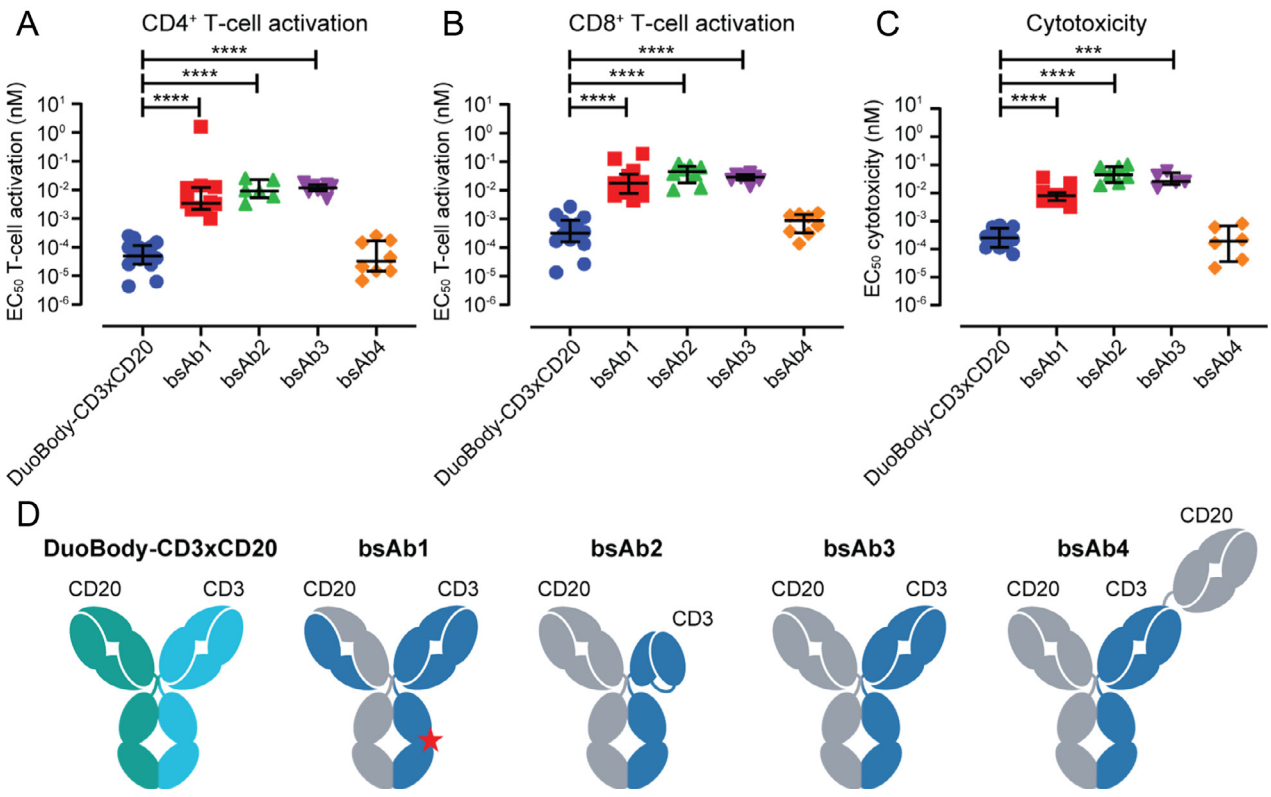

Fig. 3. *In vitro* comparison of DuoBody-CD3xCD20 with other CD3xCD20 bsAb in clinical development. **A-C:** Isolated T cells were incubated with Ab and CD20-expressing Daudi cells (E:T ratio 2:1). Percentages CD69-positive $CD4^+$ (**A**) and $CD8^+$ (**B**) cells and cytotoxic activity (**C**) were assessed by flow cytometry after 48 h. Each dot represents the EC_{50} value calculated from one experiment. Different T-cell donors were used for the individual experiments. Median EC_{50} values ± interquartile range for each antibody are indicated. **D.** Cartoon of DuoBody-CD3xCD20 and bsAb1-4. DuoBody-CD3xCD20,obtained by cFAE, is an IgG1 and contains the L234F, L235E, D265A Fc-silencing mutations; bsAb1, obtained by asymmetric reengineering technology, has a common light chain, is an IgG4 with S228P hinge stabilization and E233P-F234V-L235A-G236del Fc-silencing mutations and mutations in one of the Fc regions to purify bsAb (H435R, Y436F; indicated by star); bsAb2 is an XmAb (Fab-FcxFv-Fc) IgG1 with E233P-L234V-L235A-G236del-S267K Fc-silencing mutations, bsAb3 is a knob-into-hole IgG1 with an N297G Fc-silencing mutation, bsAb4 is a Fab-Fab-FcxFab-Fc (2:1) knob-into-hole CrossMab IgG1 with L234A-L235A-P329G Fc-silencing mutations (references for sequences of these bsAb are mentioned in the Mat & Meth section; formats are reviewed in [46]).

rituximab (IgG1-RTX), which competes with 7D8 for CD20 binding [31]. To ensure that anti-tumour activity observed in this study could be attributed to DuoBody-CD3xCD20 and not rituximab, Fc-mediated effector functions of IgG1-RTX were silenced by introducing the FEA mutations (IgG1-RTX-FEA). The presence of up to 10 mg/kg IgG1-RTX-FEA did not reduce the potency of 0.05 mg/kg DuoBody-CD3xCD20 *in vivo* (Fig. 4B). This provides a preclinical indication that patients that still have rituximab in the circulation after failing to respond to a rituximab-containing treatment regimen could still benefit from treatment with DuoBody-CD3xCD20.

The therapeutic potential of DuoBody-CD3xCD20 was assessed in HIS mice, using both an IV and a SC xenograft model [19]. In the IV tumour model, representing the leukemic phase of B-cell malignancies, mice were injected IV with Daudi cells and Ab treatment was initiated 3 days later. Treatment with DuoBody-CD3xCD20, but not the control bsAb-CD3xctrl, resulted in inhibition of tumour outgrowth (Fig. 4C). The more solid manifestation of Non-Hodgkin's lymphoma was mimicked by injecting HIS mice SC with Raji lymphoma cells and tumours were allowed to establish before Ab treatment was initiated. DuoBody-CD3xCD20 induced a profound inhibition of tumour growth at doses of 0.1 mg/kg and 1 mg/kg, whereas bsAb-CD3xctrl did not show anti-tumour activity (Fig. 4D). Interestingly, bsAb-ctrlxCD20 (but not bsAb-CD3xctrl) also induced some anti-tumour activity in this model. In addition to evaluating the anti-tumour activity of DuoBody-CD3xCD20, this HIS-model allowed the opportunity to study depletion of normal human B cells from the circulation. On day 4, 9 and 16, a significant decrease in circulating B cells was observed after treatment with DuoBody-CD3xCD20 (0.1 and 1 mg/kg) and bsAb-ctrlxCD20 ($p<0.05$) compared to the PBS-treated mice (Fig. 4E). In mice treated with 1 mg/kg DuoBody-CD3xCD20, but not bsAb-ctrlxCD20, a transient upregulation of the T-cell activation marker CD69 was observed in peripheral blood $CD4^+$ and $CD8^+$ *T* cells at day 4 (Fig. 4F, G).

In summary, DuoBody-CD3xCD20 induced anti-tumour activity *in vivo* towards malignant B cells at SC sites as well as in the blood circulation. This was accompanied by a transient T-cell activation and was not hampered by the presence of circulating rituximab.

3.5. DuoBody-CD3xCD20 induced potent and long-lasting B-cell depletion in cynomolgus monkeys after IV or SC administration

As part of the non-clinical safety studies, DuoBody-CD3xCD20 was administered to cynomolgus monkeys, the selected toxicology species for which antigen binding characteristics and *in vitro* pharmacology of DuoBody-CD3xCD20 were comparable to humans (data not shown). A single injection of DuoBody-CD3xCD20, administered IV or SC, induced a dose-dependent depletion of B cells from peripheral blood (Fig. 5A, C) and lymph nodes (Fig. 5B, D). B-cell depletion was reversible at all dose levels, with time to recovery correlating with the treatment dose. Efficiency of B-cell depletion was comparable after SC and IV administration.

Analysis of DuoBody-CD3xCD20 levels in plasma demonstrated different PK profiles for the IV and SC administration routes. Following IV infusion, the peak plasma concentration (C_{max}) was reached at the end of the 30-min dosing period, to then decrease in a generally bi-phasic manner (Fig. 5E). After SC dosing, C_{max} was not reached until approximately three days after dosing and the plasma levels remained relatively steady up to seven days post dose. Thereafter,

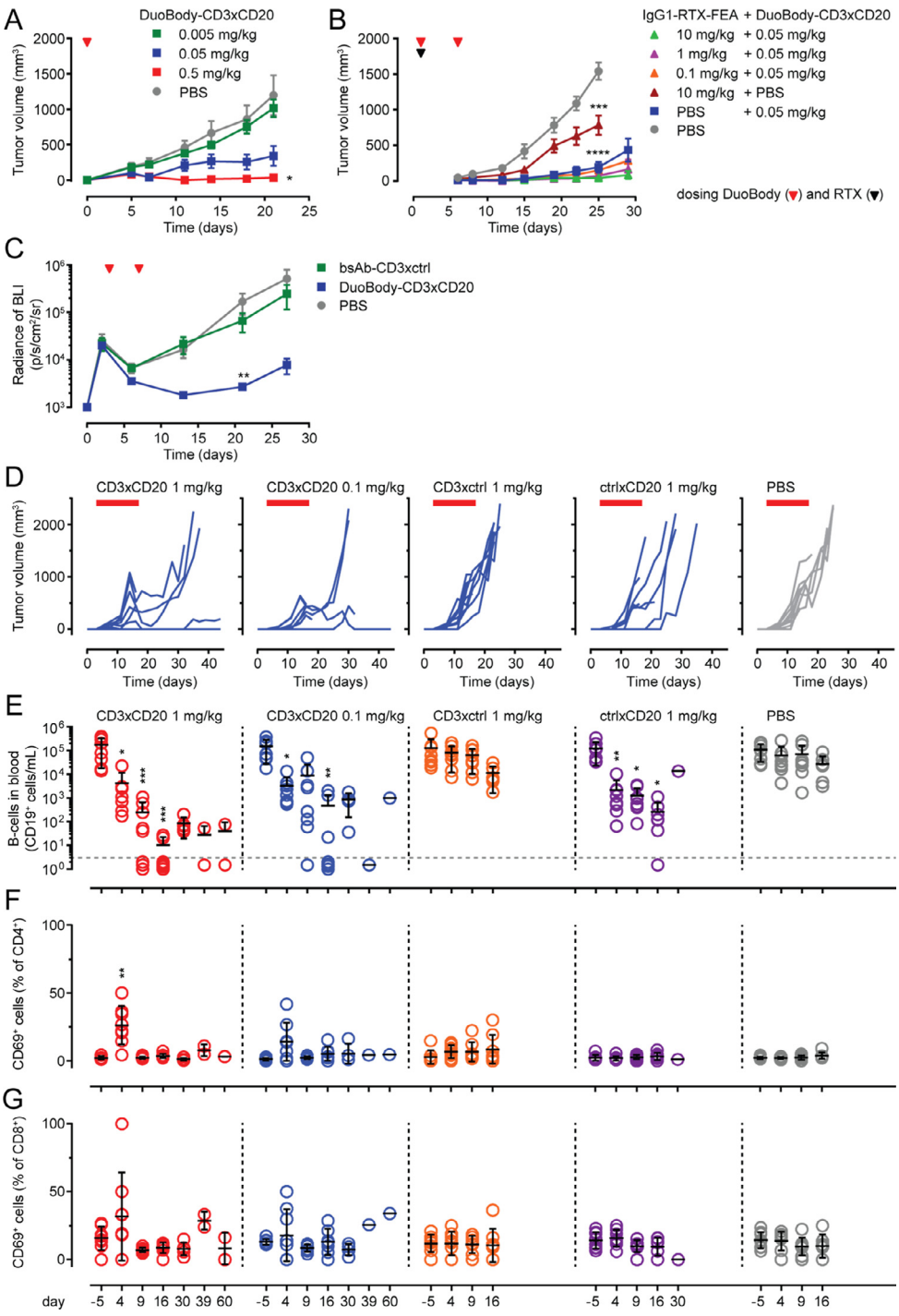

Fig. 4. Anti-tumour activity of DuoBody-CD3xCD20 *in vivo* in humanized mouse models. **A-B:** Tumours were induced in NOD-SCID mice by SC injection of a 1:1 mixture of human PBMC and Raji-luc cells at day 0. Immediately after tumour inoculation, mice (5 per group) were treated with a single IV dose of DuoBody-CD3xCD20 (0.5, 0.05, 0.005 mg/kg) (**A**) or mice (10 per group) were given a single IV dose of IgG1-RTX-FEA (10, 1 or 0.1 mg/kg), followed by IV treatment with 0.05 mg/kg DuoBody-CD3xCD20 4 h later, treatment with DuoBody-CD3xCD20 was repeated on day 7 (**B**). Data shown are mean tumour volumes per treatment group ± SEM. Differences were analysed by Mann-Whitney two-tailed test *versus* PBS (A: day 21; B: day 25). Statistically significant differences are indicated as follows: * $p < 0.05$, *** $p < 0.0005$, **** $p < 0.0001$ (**A-B**). **C:** Tumours were induced in BRGS-HIS mice by IV injection of Daudi-luc cells at day 0. Mice were treated IV with 1 mg/kg DuoBody-CD3xCD20 on day 3 and day 7. Tumour growth was evaluated by BLI and depicted as average radiance of BLI ± SEM (7 mice per group). Statistically significant differences compared to PBS-treated mice were determined by Kruskal-Wallis ANOVA test followed by Dunn's multiple comparison post-test (** $p < 0.01$). **D-G:** Tumours were induced in BRGS-HIS mice by SC injection of Raji-luc cells at day 0. Mice were treated IV with 1 mg/kg or 0.1 mg/kg bsAb or vehicle control on days 3, 7, 10, 14, and 17. Tumour growth is shown for each individual mouse, one graph per treatment group (**D**). Individual (circles) and average (black line) absolute numbers of circulating human CD19⁺ *B* cells determined by flow cytometry at indicated time points (**E**). T-cell activation was determined on indicated time points by flow cytometry. Individual (circles) and average (black line) percentages of CD69⁺ cells in CD4⁺ *T*-cell population (**F**) and CD8⁺ *T*-cell population (**G**) are shown. Statistically significant differences compared to PBS-treated mice at each time point were determined by Kruskal-Wallis ANOVA test with Dunn's multiple comparisons test (* $p < 0.05$, ** $p < 0.01$, *** $p < 0.001$) (**E-G**).

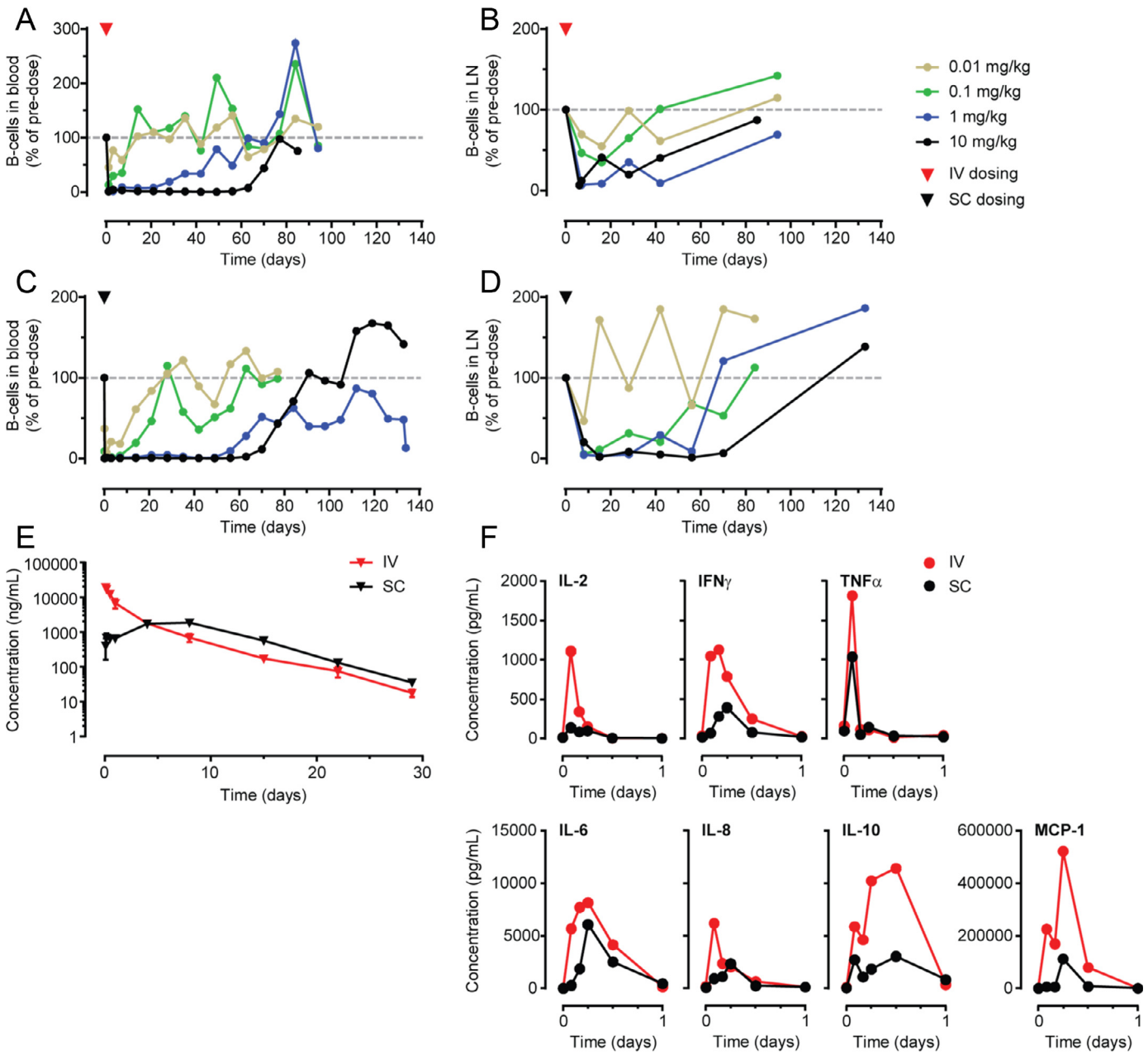

Fig. 5. Anti-B-cell activity of DuoBody-CD3xCD20 in cynomolgus monkeys after IV and SC administration. **A-D:** B-cell counts ($CD19^+$ cells) are depicted per monkey (n = 2 per dose group) as a percentage of the B-cell counts prior to dosing. B-cell counts in peripheral blood (**A, C**) and lymph nodes (**B, D**) were measured by flow cytometry and are shown for the indicated dose levels of a single IV (**A, B**) or SC (**C, D**) administration of DuoBody-CD3xCD20. **E**: Mean ± SEM plasma concentration profiles for DuoBody-CD3xCD20 measured by Single Molecule Counting ImmunoAssay (SMCIA) after a single IV or SC dose of 1 mg/kg DuoBody-CD3xCD20 (6 monkeys/group). **F**: Mean plasma concentration profiles of indicated cytokines measured after a single IV or SC dose of 1 mg/kg DuoBody-CD3xCD20 (6 monkeys/group).

concentrations decreased in a mono-phasic manner up to the end of the four-week sampling period. At doses of 0.1 and 1 mg/kg DuoBody-CD3xCD20, the peak plasma concentration was 7- to 17-fold higher after IV compared to SC dosing. Importantly, the exposure (area under the curve) of a single dose of 0.1 or 1.0 mg/kg was comparable after SC and IV injection.

Injection of DuoBody-CD3xCD20 was associated with a rapid and transient increase in plasma cytokine levels. Interleukin (IL)−2, IL-6, IL-8, IL-10, interferon (IFN)γ, tumour necrosis factor (TNF)α and monocyte chemoattractant protein (MCP)−1 reached peak levels within 2−12 h after dosing (Fig. 5F) and had resolved to baseline after 24 h. Peak cytokine levels were considerably lower after SC compared to IV treatment. For IL-6, IL-8 and IFNγ peak cytokine levels were reached somewhat later after SC compared to IV dosing, although for both administration routes plasma levels had returned to baseline at 12−24 h.

In summary, DuoBody-CD3xCD20 induced profound and long-lasting depletion of B cells from peripheral blood and lymph nodes in cynomolgus monkeys, with comparable efficacy between IV and SC administration. Peak plasma levels of DuoBody-CD3xCD20 were reduced after SC administration compared to IV administration and SC administration was associated with reduced plasma cytokine levels.

3.6. Discussion

DuoBody-CD3xCD20 (GEN3013) is a new bsAb recognizing CD3 and CD20, that triggers highly potent T-cell-mediated lysis of CD20-expressing cells. DuoBody-CD3xCD20 is a full-length IgG1 bsAb generated by cFAE of a humanized version of mouse anti-human CD3 mAb SP34 and human anti-CD20 mAb 7D8. Fc-mediated effector functions were silenced by the introduction of three amino acid mutations (FEA) in the

Fc region. *In vitro*, DuoBody-CD3xCD20 induced potent and specific activation and cytotoxic activity of both $CD4^+$ and $CD8^+$ *T* cells. Although activation of $CD4^+$ and $CD8^+$ *T* cells by DuoBody-CD3xCD20 was detected at similar bsAb concentrations and in a comparable timeframe, $CD8^+$ *T* cells induced cytotoxic activity faster than $CD4^+$ *T* cells. This has been described previously [32] and most likely reflects an intrinsic difference between T-cell subtypes: whereas $CD8^+$ *T* cells are harnessed with granules containing cytotoxic molecules that can be released immediately upon activation, $CD4^+$ *T* cells are not primarily cytotoxic and first need to produce cytotoxic molecules in order to exert cytotoxic activity [33]. It would be highly interesting to gain further understanding of the contribution of $CD4^+$ and $CD8^+$ *T*-cell populations in the clinical setting.

Intriguingly, DuoBody-CD3xCD20 induced T-cell activation and cytotoxicity with EC_{50} values in the low ng/mL (low picomolar) range, whereas EC_{50} values for binding to CD20 on B cells and CD3 on T cells were roughly 1000-fold higher (μg/mL range). This shows that efficient T-cell-mediated cytotoxicity can be achieved when TAA binding is far from saturated, and is in line with studies demonstrating efficient CD3 bsAb-induced T-cell-mediated killing, even if antigen expression levels are very low [34–37]. This might be promising for treatment of patients with malignancies with lower CD20 expression levels, such as ALL. A low antigen expression threshold for CD3 bsAb is also in agreement with lack of correlation between CD20 expression levels and DuoBody-CD3xCD20-induced T-cell-mediated cytotoxicity, an observation that has previously been described for CD3 bsAb targeting other TAAs [34,36].

The cytotoxic capacity of CD3 bsAb is determined by the characteristics of its two Fab arms and by characteristics of the TAA. However, the exact characteristics determining CD3 bsAb potency are poorly understood. To understand the highly potent cytotoxicity of DuoBody-CD3xCD20, we looked at the relation between the expression of a diverse panel of B-cell antigens, and the cytotoxic activity of CD3 bsAb targeting those antigens. Differences in expression levels between the different B-cell antigens could not predict the potency of CD3 bsAb, in line with the lack of correlation between antigen expression and CD3 bsAb potency for specific target antigens ([34,36] and the present study). For example, CD3 bsAb targeting HLA-DR and CD138, both of which show expression levels sufficient for cytotoxic activity of CD3 bsAb targeting the other B-cell antigens, did not induce killing of B cells. This lack of cytotoxicity can likely be attributed to other target antigen characteristics. For HLA-DR it can be speculated that the immune synapse formation between B and T cells is disrupted by the bsAb due to steric hindrance. Moreover, it cannot be excluded that lack of cytotoxicity for HLA-DR-specific CD3 bsAb might be caused by expression of HLA-DR on activated T cells [38], causing fratricide [39].

Zooming in on CD3 bsAb targeting CD20, CD37 and CD70, no correlation was observed between antigen binding affinity and (fine) binding domain specificity of CD3 bsAb and cytotoxic activity. This was unexpected, since previous studies demonstrated a correlation between CD3 bsAb efficacy and localization of the binding epitope on the TAA [40,41]. While the CD20, CD37 and CD70 bsAb studied here showed diversity in binding epitopes, the panel of CD3 bsAb explored for each antigen was small and more detailed studies may provide better insight in the binding epitope requirements for CD3 bsAb targeting these antigens. In addition to the characteristics studied here, other factors may contribute to CD3 bsAb potency, including the bsAb format [42], and TAA characteristics such as molecular size [41], flexibility [40], mobility [43], macromolecular organization [43], accessibility, ease of formation of an immunological synapse, and expression of costimulatory and coinhibitory receptors on the tumour cells, making it nearly impossible to rationalize target antigen and epitope choices. In summary, the high potency of DuoBody-CD3xCD20 in T-cell-mediated targeting of B cells, which was also illustrated by the comparison with four other CD3xCD20 bsAb that are in clinical development, could not have been predicted based on the known characteristics of the 7D8 Ab clone and CD20.

DuoBody-CD3xCD20 showed potent anti-tumour activity in lymphoma xenograft models in humanized mice, also in the presence of a large excess of circulating rituximab, which competes with 7D8 for CD20 binding [31]. Again, this illustrates that probably only a very small amount of available antigen is required for CD3 bsAb to exert optimal activity. From a clinical perspective, efficacy of DuoBody-CD3xCD20 in the presence of rituximab may indicate that patients that still have CD20 mAb in the circulation when they are no longer responding to CD20 mAb-containing treatments, could be eligible for treatment with DuoBody-CD3xCD20. Surprisingly, we also observed some *in vivo* anti-tumour activity of a control bsAb containing the CD20-binding Fab arm and a non-binding Fab-arm instead of the CD3-binding Fab arm (bsAb-ctrlxCD20). This is remarkable, because of the inert Fc region, but a similar effect was observed using a rituximab variant carrying the FEA mutations. Any residual interaction of human IgG1 molecules carrying the FEA mutations with mouse FcγRIV, which has been shown to be the dominant mouse FcγR in antibody-mediated anti-tumour activity *in vivo* [44], was excluded (Genmab, unpublished data). Although the mechanism behind this CD20-specific Fab-mediated effect on tumour growth needs further investigation, it may contribute to the potent anti-tumour activity of DuoBody-CD3xCD20.

Blinatumomab, the only FDA-approved CD3 bsAb, is a fragment-based bsAb targeting CD19, currently approved for the treatment of B-cell precursor ALL. Because of the lack of an Fc region, the half-life of blinatumomab in humans is short, necessitating continuous IV infusion [45]. DuoBody-CD3xCD20 has a regular IgG1 structure and biochemical characteristics typical of a human IgG1 antibody, including a relatively long plasma half-life. The Fc region of DuoBody-CD3xCD20 contains three mutations (L234F, L235E, D265A) to abrogate FcγR and complement binding, thereby preventing the induction of T-cell activation through antibody-mediated, FcγR-dependent CD3 crosslinking and ensuring that T-cell activation is strictly dependent on simultaneous binding of CD3 and CD20. Binding to FcRn is not affected by the mutations. Neurotoxicities, as observed for blinatumomab, have been described for other CD19-targeting T-cell therapies and are thought to be class-related [45]. It would be interesting to see comparison of the clinical safety profile of blinatumomab and DuoBody-CD3xCD20, but at present insufficient clinical data is available.

In nonclinical safety studies in cynomolgus monkeys, DuoBody-CD3xCD20 induced profound depletion of B cells from both peripheral blood and lymph nodes, which was comparable after IV and SC administration. While bioavailability was comparable between the administration routes, peak plasma levels were lower and delayed after SC administration. Importantly, peak cytokine levels were consistently lower after SC administration. In the clinic, cytokine release and associated adverse events are an important concern for CD3 bsAb, therefore the SC administration route could provide a method to reduce cytokine release in patients.

In conclusion, DuoBody-CD3xCD20 (GEN3013) is a new bsAb that showed specific and highly potent preclinical anti-tumour activity in lymphoma models *in vitro* and *in vivo*. DuoBody-CD3xCD20 induced profound depletion of B cells from peripheral blood and lymphoid organs in cynomolgus monkeys upon IV or SC administration, with lower levels of plasma cytokines observed after SC compared to IV administration. These preclinical studies provided the rationale to assess the clinical safety and efficacy of subcutaneous administration of DuoBody-CD3xCD20 (GEN3013) in patients with relapsed, progressive or refractory B-cell lymphoma (GCT3013-01, NCT03625037).

Acknowledgements

The authors would like to thank Bart-Jan de Kreuk for supporting the Ab Fc-silencing studies, Kieshen Kalloe, Marcel Brandhorst and Jeroen van den Brakel for technical support for *in vivo* efficacy studies, and Ilse Somers for supporting mouse PK studies.

Funding Sources: Genmab

Declaration of competing interest

(former) Genmab employees own Genmab warrants and/or stock. PJE reports to be inventor on patent (application) WO2016/110576; JM reports to be inventor on patent (application) WO2011/131746, WO2014/108483, WO2015/001085; JN reports to be inventor on patent (application) WO2011/131746, WO2014/108483, and WO2015/001085; ENvdB reports to be inventor on patent (application) WO2014/108483, WO2015/001085, and WO2016/110576; SV reports to be inventor on patent (application) WO2016/110576; AFL reports to be inventor on patent (application) WO2011/131746, WO2014/108483, WO2015/001085; JS reports to be inventor on patent (application) WO2011/131746, WO2014/108483, WO2015/001085, WO2016/110576; PWHIP reports to be inventor on patent (application) WO2004/035607, WO2011/131746, WO2014/108483, WO2015/001085, WO2016/110576 and to be employed by Lava Therapeutics and ECWB reports to be inventor on patent (application) WO2016/110576.

Author contributions

Patrick J. Engelberts: Designed and performed experiments, analysed data, wrote manuscript
Ida H. Hiemstra: designed experiments, analysed data, wrote manuscript
Bart de Jong: performed experiments, analysed data
Danita H. Schuurhuis: wrote manuscript
Joyce Meesters: performed experiments, analysed data
Irati Beltran Hernandez: performed experiments
Simone C. Oostindie: performed experiments
Joost Neijssen: designed experiments, analysed data
Edward N. van den Brink: designed experiments, analysed data
Sjeng Horbach: designed non-clinical safety studies in monkeys, analysed data
Sandra Verploegen: designed *in vivo* studies in mice, analysed data
Aran F. Labrijn: designed pharmacology experiments, analysed data
Theodora Salcedo: designed non-clinical safety studies in monkeys
Janine Schuurman: supervision
Paul W.H.I Parren: designed experiments, wrote manuscript, supervision
Esther C.W. Breij: designed experiments, analysed data, supervision

Supplementary materials

Supplementary material associated with this article can be found in the online version at doi:10.1016/j.ebiom.2019.102625.

References

[1] Guerra VA, Jabbour EJ, Ravandi F, Kantarjian H, Short NJ. Novel monoclonal antibody-based treatment strategies in adults with acute lymphoblastic leukemia. Ther Adv Hematol 2019;10:2040620719849496.
[2] Huguet F, Tavitian S. Emerging biological therapies to treat acute lymphoblastic leukemia. Expert Opin Emerg Drugs 2017;22:107–21.
[3] Owen CJ, Stewart DA. Obinutuzumab for B-cell malignancies. Expert Opin Biol Ther 2014;14:1197–205.
[4] Gisselbrecht C, Glass B, Mounier N, et al. Salvage regimens with autologous transplantation for relapsed large B-cell lymphoma in the rituximab era. J Clin Oncol 2010;28:4184–90.
[5] Johnson NA, Leach S, Woolcock B, et al. CD20 mutations involving the rituximab epitope are rare in diffuse large B-cell lymphomas and are not a significant cause of R-Chop failure. Haematologica 2009;94:423–7.
[6] Offner S, Hofmeister R, Romaniuk A, Kufer P, Baeuerle PA. Induction of regular cytolytic T cell synapses by bispecific single-chain antibody constructs on MHC class I-negative tumor cells. Mol Immunol 2006;43:763–71.
[7] Labrijn AF, Meesters JI, de Goeij BE, et al. Efficient generation of stable bispecific IgG1 by controlled Fab-arm exchange. Proc Natl Acad Sci USA 2013;110:5145–50.
[8] Labrijn AF, Meesters JI, Priem P, et al. Controlled Fab-arm exchange for the generation of stable bispecific IgG1. Nat Protoc 2014;9:2450–63.
[9] Gramer MJ, van den Bremer ET, van Kampen MD, et al. Production of stable bispecific IgG1 by controlled Fab-arm exchange: scalability from bench to large-scale manufacturing by application of standard approaches. MAbs 2013;5:962–73.
[10] Teeling JL, French RR, Cragg MS, et al. Characterization of new human CD20 monoclonal antibodies with potent cytolytic activity against non-Hodgkin lymphomas. Blood 2004;104:1793–800.
[11] Teeling JL, Mackus WJ, Wiegman LJ, et al. The biological activity of human CD20 monoclonal antibodies is linked to unique epitopes on CD20. J Immunol 2006;177:362–71.
[12] Vink T, Oudshoorn-Dickmann M, Roza M, Reitsma JJ, de Jong RN. A simple, robust and highly efficient transient expression system for producing antibodies. Methods 2014;65:5–10.
[13] Burton DR, Pyati J, Koduri R, et al. Efficient neutralization of primary isolates of HIV-1 by a recombinant human monoclonal antibody. Science 1994;266:1024–7.
[14] Rodrigues ML, Shalaby MR, Werther W, Presta L, Carter P. Engineering a humanized bispecific F(ab')2 fragment for improved binding to T cells. Int J Cancer Suppl 1992;7:45–50.
[15] Overdijk MB, Verploegen S, van den Brakel JH, et al. Epidermal growth factor receptor (EGFR) antibody-induced antibody-dependent cellular cytotoxicity plays a prominent role in inhibiting tumorigenesis, even of tumor cells insensitive to EGFR signaling inhibition. J Immunol 2011;187:3383–90.
[16] Da Roit F, Engelberts PJ, Taylor RP, et al. Ibrutinib interferes with the cell-mediated anti-tumor activities of therapeutic CD20 antibodies: implications for combination therapy. Haematologica 2015;100:77–86.
[17] Schneider CA, Rasband WS, Eliceiri KW. NIH Image to ImageJ: 25 years of image analysis. Nat Methods 2012;9:671–5.
[18] Brischwein K, Schlereth B, Guller B, et al. MT110: a novel bispecific single-chain antibody construct with high efficacy in eradicating established tumors. Mol Immunol 2006;43:1129–43.
[19] Legrand N, Huntington ND, Nagasawa M, et al. Functional CD47/signal regulatory protein alpha (SIRP(alpha)) interaction is required for optimal human T- and natural killer- (NK) cell homeostasis *in vivo*. Proc Natl Acad Sci USA 2011;108:13224–9.
[20] Labrijn AF, Meesters JI, Bunce M, et al. Efficient generation of bispecific murine antibodies for pre-clinical investigations in syngeneic rodent models. Sci Rep 2017;7:2476.
[21] Canfield SM, Morrison SL. The binding affinity of human IgG for its high affinity Fc receptor is determined by multiple amino acids in the CH2 domain and is modulated by the hinge region. J Exp Med 1991;173:1483–91.
[22] Duncan AR, Winter G. The binding site for C1q on IgG. Nature 1988;332:738–40.
[23] Duncan AR, Woof JM, Partridge LJ, Burton DR, Winter G. Localization of the binding site for the human high-affinity Fc receptor on IgG. Nature 1988;332:563–4.
[24] Idusogie EE, Presta LG, Gazzano-Santoro H, et al. Mapping of the C1q binding site on rituxan, a chimeric antibody with a human IgG1 Fc. J Immunol 2000;164:4178–84.
[25] Oganesyan V, Gao C, Shirinian L, Wu H, Dall'Acqua WF. Structural characterization of a human Fc fragment engineered for lack of effector functions. Acta Crystallogr D Biol Crystallogr 2008;64:700–4.
[26] Shields RL, Namenuk AK, Hong K, et al. High resolution mapping of the binding site on human IgG1 for Fc gamma RI, Fc gamma RII, Fc gamma RIII, and FcRn and design of IgG1 variants with improved binding to the Fc gamma R. J Biol Chem 2001;276:6591–604.
[27] Tao MH, Morrison SL. Studies of aglycosylated chimeric mouse-human IgG. Role of carbohydrate in the structure and effector functions mediated by the human IgG constant region. J Immunol 1989;143:2595–601.
[28] Pessano S, Oettgen H, Bhan AK, Terhorst C. The T3/T cell receptor complex: antigenic distinction between the two 20-kd T3 (T3-delta and T3-epsilon) subunits. EMBO J 1985;4:337–44.
[29] Teeling JL, Mackus WJ, Wiegman LJ, et al. The biological activity of human CD20 monoclonal antibodies is linked to unique epitopes on CD20. J Immunol 2006;177:362–71.
[30] Polyak MJ, Deans JP. Alanine-170 and proline-172 are critical determinants for extracellular CD20 epitopes; heterogeneity in the fine specificity of CD20 monoclonal antibodies is defined by additional requirements imposed by both amino acid sequence and quaternary structure. Blood 2002;99:3256–62.
[31] Engelberts PJ, Badoil C, Beurskens FJ, et al. A quantitative flow cytometric assay for determining binding characteristics of chimeric, humanized and human antibodies in whole blood: proof of principle with rituximab and of atumumab. J Immunol Method 2013;388:8–17.
[32] Mack M, Gruber R, Schmidt S, Riethmuller G, Kufer P. Biologic properties of a bispecific single-chain antibody directed against 17-1A (EpCAM) and CD3: tumor cell-dependent T cell stimulation and cytotoxic activity. J Immunol 1997;158:3965–70.
[33] Grossman WJ, Verbsky JW, Tollefsen BL, Kemper C, Atkinson JP, Ley TJ. Differential expression of granzymes A and B in human cytotoxic lymphocyte subsets and T regulatory cells. Blood 2004;104:2840–8.
[34] Friedrich M, Henn A, Raum T, et al. Preclinical characterization of AMG 330, a CD3/CD33-bispecific T-cell-engaging antibody with potential for treatment of acute myelogenous leukemia. Mol Cancer Ther 2014;13:1549–57.
[35] Lopez-Albaitero A, Xu H, Guo H, et al. Overcoming resistance to HER2-targeted therapy with a novel HER2/CD3 bispecific antibody. Oncoimmunology 2017;6:e1267891.
[36] Oberst MD, Fuhrmann S, Mulgrew K, et al. CEA/CD3 bispecific antibody MEDI-565/AMG 211 activation of T cells and subsequent killing of human tumors is independent of mutations commonly found in colorectal adenocarcinomas. MAbs 2014;6:1571–84.
[37] Xu H, Cheng M, Guo H, Chen Y, Huse M, Cheung NK. Retargeting T cells to GD2 pentasaccharide on human tumors using Bispecific humanized antibody. Cancer Immunol Res 2015;3:266–77.

[38] Tomkinson BE, Wagner DK, Nelson DL, Sullivan JL. Activated lymphocytes during acute Epstein-Barr virus infection. J Immunol 1987;139:3802–7.
[39] Leisegang M, Wilde S, Spranger S, et al. MHC-restricted fratricide of human lymphocytes expressing survivin-specific transgenic T cell receptors. J Clin Invest 2010;120:3869–77.
[40] Bluemel C, Hausmann S, Fluhr P, et al. Epitope distance to the target cell membrane and antigen size determine the potency of T cell-mediated lysis by BiTe antibodies specific for a large melanoma surface antigen. Cancer Immunol Immunother 2010;59:1197–209.
[41] Li J, Stagg NJ, Johnston J, et al. Membrane-Proximal epitope facilitates efficient T cell synapse formation by Anti-FcRH5/CD3 and is a requirement for myeloma cell killing. Cancer Cell 2017;31:383–95.
[42] Moore PA, Zhang W, Rainey GJ, et al. Application of dual affinity retargeting molecules to achieve optimal redirected T-cell killing of B-cell lymphoma. Blood 2011;117:4542–51.
[43] Pfosser A, Brandl M, Salih H, Grosse-Hovest L, Jung G. Role of target antigen in bispecific-antibody-mediated killing of human glioblastoma cells: a pre-clinical study. Int J Cancer 1999;80:612–6.
[44] Nimmerjahn F, Lux A, Albert H, et al. FcgammaRIV deletion reveals its central role for IgG2a and IgG2b activity *in vivo*. Proc Natl Acad Sci USA 2010;107:19396–401.
[45] Friberg G, Blinatumomab Reese D. (Blincyto): lessons learned from the bispecific t-cell engager (BiTE) in acute lymphocytic leukemia (ALL). Ann. Oncol. 2017;28:2009–12.
[46] Labrijn AF, Janmaat ML, Reichert JM, Parren P. Bispecific antibodies: a mechanistic review of the pipeline. Nat Rev Drug Discov. 2019;18:585–608.